PAPER

Check for updates

Tribocatalytic degradation of concentrated methyl orange solutions by BiFeO₃ nanoparticles prepared through a sol–gel method

Yanhong Gu, [ID] [a] Weiying Zhang,[a] Yuen Li, [ID] [a] Kelan Wang, [ID] [a] Lanlan Ge, [ID] [a] Xianghui Zhang, [ID] [a] Jianguo Zhao,[a] Zhenjiang Shen, [ID] [b] Wanping Chen[c] and Yaohua Hu *[a]

With a relatively narrow bandgap of around 2.0 eV, BiFeO₃ (BFO) nanoparticles have been extensively investigated as an appealing visible-light photocatalyst. In this study, BFO nanoparticles prepared through a sol–gel method were explored as a tribocatalyst to degrade methyl orange (MO) solutions. With BFO nanoparticles stimulated through magnetic stirring using Teflon magnetic rotary disks, as much as 100% of 10 mg per L MO and 99% of 30 mg per L MO solutions were degraded after 20 min and 160 min of magnetic stirring, respectively. For reference, TiO₂ nanoparticles (P25) were stimulated under the same conditions and degraded 97% of 10 mg per L MO and 97% of 30 mg per L MO solutions after 150 min and 540 min of magnetic stirring, respectively. The calculated MO degradation rate constants for BFO at concentrations of 10 mg per L and 30 mg per L were 4.94 h⁻¹ and 1.19 h⁻¹, respectively, while the corresponding values for P25 were 0.86 h⁻¹ and 0.40 h⁻¹, respectively. Free radical trapping experiments showed that positive holes are by far the most important active species in the tribocatalytic degradation of MO by BFO. These findings suggest that in addition to its versatile applications, multiferroic BFO is promising for converting mechanical energy into chemical energy through tribocatalysis.

1. Introduction

The extensive use of fossil fuels has not only resulted in the escalating depletion of fossil fuels but has also detrimentally impacted the global environment.[1,2] In recent years, there has been a growing emphasis on technologies able to capture and use renewable energies from nature,[3,4] including thermal, solar, chemical, mechanical, and biological energy. Photocatalysis is a well-known technology for absorbing solar light and converting it into chemical energy, in which electron–hole pairs are excited in semiconductors upon light irradiation and subsequently induce various redox reactions.[5–7] The photocatalytic treatment of various pollutants has become a research hotspot in the past decade.[8–12] However, owing to the inherent instability of solar light and the limited effectiveness of promising photocatalysts, photocatalysis alone is insufficient to provide a satisfactory solution to environmental pollution.[13–15]

Similar to solar light, mechanical energy is a renewable source of energy widely available in nature.[4,7] While mechanical energy derived from rivers, winds and tides has been mostly converted into electricity to date, there has been a growing interest in harnessing natural mechanical energy for environmental remediation in recent years, which has inspired the development of some novel technologies.[13,16–18] In 2019, Li *et al.* first reported the tribocatalytic degradation of organic dyes by Ba₀.₇Sr₀.₂₅TiO₃ nanoparticles,[19] which marks the beginning of the utilization of mechanical energy through friction for environmental remediation. Subsequently, numerous other materials, such as BaTiO₃,[7,20–22] FeS₂,[23] ZnO,[16,24] BiOIO₃,[13] Bi₂WO₆,[25,26] SrTiO₃,[24] TiO₂,[17,27] and CdS[22] were explored for the tribocatalytic degradation of organic dyes, and some encouraging results were obtained. The source of friction catalysis was initially mechanical stirring using Teflon magnetic stir bars. To investigate the efficiency of friction catalysis, the number of Teflon magnetic stir bars was increased.[13,19] In 2022, Cui *et al.* proposed replacing Teflon magnetic stir bars with rotating discs, which significantly enhanced the efficiency of friction catalysis.[27] The test methods are ultimately identified and discussed on the basis of the catalytic degradation efficiency of the dyes.

Considering the above-mentioned materials, it can be seen that many materials that have been investigated in tribocatalysis are semiconductors.[28] As a matter of fact, a mechanism

ᵃSchool of Physics and Electronic Information and Key Lab Electromagnet Transformat&Detect Henan, Luoyang Normal College, Luoyang 471022, Henan, P. R. China. E-mail: huyaohua1@sina.com

ᵇCollege of Physics and Electronic Engineering, Hainan Normal University, Hainan 571158, China

ᶜSchool of Physics and Technology, Wuhan University, Wuhan 430072, China

based on the excitation of electron–holes pairs in semi-conductors by mechanical energy absorbed through friction has been proposed for tribocatalysis.[17,19] This implies the importance of materials with a semiconductor-type bandgap in tribocatalysis.[4,13] $BiFeO_3$, a well-known multiferroic material, has a narrow bandgap of 2.0 eV.[6] BFO has demonstrated significant potential in the photocatalytic breakdown of water pollutants[9,12] and the construction of heterojunction photocatalytic water splitting for hydrogen production. This is attributed to its outstanding crystal structure characteristics and ability to be activated under visible light for photocatalytic processes.[29,30] In this study, BFO nanoparticles were prepared through a sol–gel method, and their potential in environmental remediation was evaluated in terms of the tribocatalytic degradation of methyl orange (MO) solutions. To our great surprise, stimulated by magnetic stirring using Teflon magnetic rotary disks,[27] they degraded 99% of 30 mg per L MO in 180 min, with a degradation rate constant three times that of P25, an important commercial photocatalyst. It is well known that MO molecules possess high-energy bonds, and the degradation of a concentrated MO solution is highly challenging.[25,31,32] These findings suggest that in addition to its numerous known uses, BFO exhibits a promising role in environmental remediation *via* tribocatalysis.

2. Experimental procedures

2.1 Material preparation and characterization

All raw materials were purchased from Shanghai Aladdin Biochemical Technology Co., Ltd. At 50 °C, 0.02 mol of Fe $(NO_3)_3$ $9H_2O$ (99%) and 0.021 mol of Bi $(NO_3)_3 5H_2O$ (99%) were added to 20 mL of ethylene glycol solution and stirred for 1.5 h. The mixture was left to settle for a while and then placed in an oven to dry at 100 °C for 48 h, followed by heating in a horizontal tube furnace at 600 °C in air for 3 h, and finally cooled to room temperature. For comparison, P25, a commercially available photocatalyst consisting of 30 nm titanium dioxide nanoparticles, was obtained from Degussa Chemical Company.

The X-ray diffraction (XRD) patterns of the samples were obtained using an X-ray diffractometer (Smartlab-9) using Cu K_α radiation. The microstructures were analyzed through a scanning electron microscope (Inspect F50). The sample bandgap width was measured using UV-visible analysis (UV-2550; Shimadzu, Kyoto, Japan).

2.2 Tribocatalytic degradation of MO solutions

First, 0.3 g of bismuth ferrite powder or P25 was added to 30 mL of methyl orange solution in a glass beaker of Φ 40 × 50 mm. Next, a homemade Teflon magnetic rotary disk (described in details in a previous paper[27]) was placed in the beaker to stir the suspension at 400 rpm through a magnetic stirrer. The beaker was kept in the dark, and room temperature was maintained at 20 °C. Next, 1 mL of the suspension was sampled at specific intervals, and a clear solution was obtained through centrifugation. The concentration of MO was determined through UV-visible analysis (UV-2550; Shimadzu, Kyoto, Japan).

2.3 Identification of active substances

The scavengers 0.03 mmol *p*-benzoquinone (BQ), 0.03 mmol disodium ethylenediaminetetraacetic acid salt (EDTA-2Na), 0.03 mmol *tert*-butanol (TBA), and 0.03 mmol $AgNO_3$ were introduced into beakers containing 300 mg of BFO nanoparticles and 30 mL of MO solution to capture $\cdot O^{2-}$ radicals, h^+, $\cdot OH$ radicals, and electrons, respectively. Subsequently, employing identical conditions as those in the dye degradation experiment allowed us to evaluate the catalytic effect caused by friction on dye degradation.

3. Results and discussions

The sol–gel method is widely adopted for the preparation of pure-phase BFO nanopowders at low temperature.[33] Fig. 1a shows a representative XRD pattern of the BFO powder prepared using the sol–gel method in this study. The peaks (012), (104), (110), (202) and (024) closely match those of the standard PDF#86-1518 card for the perovskite structure BFO; from this, it can be seen that the BFO nanoparticles prepared using the sol–gel method have already formed a perovskite structure. No peaks from other phases were observed, indicating that the BFO nanoparticles had high phase purity. An electron microscopy image of BFO is shown in Fig. 1b. The average size and standard deviation of the sample grain size are 95.2 ± 32.0 nm, which is
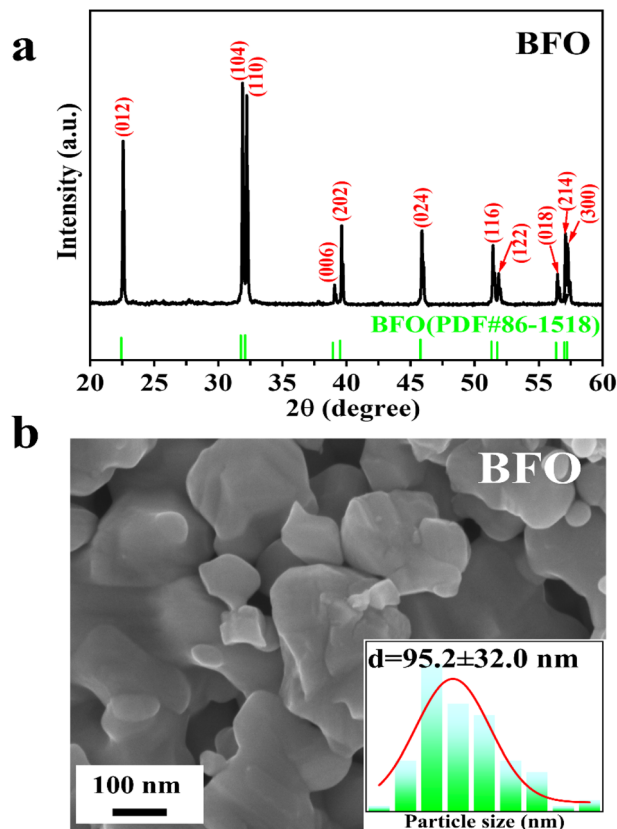

Fig. 1 BFO nanoparticles prepared in this study: (a) XRD pattern; (b) SEM image (insert map of grain distribution).

typical for BFO nanoparticles prepared through the sol–gel method.[30,33]

Being chemically stable, non-toxic, and inexpensive, P25 is an important commercial photocatalyst with wide-ranging applications.[34–36] In recent years, P25 has also been recognized as a standard tribocatalyst for environmental remediation.[17,27] As illustrated in Fig. 2a, when 10 mg per L MO solution suspended with P25 was magnetically stirred using a Teflon magnetic rotary disk, the absorbance peak at 464 nm in the ultraviolet-visible absorption spectrum decreased steadily with an increasing stirring time, and the color of the solution faded

simultaneously, as illustrated in the inset. The degradation rate of a dye is usually calculated using the formula $D = 1 - A/A_0$, where A_0 represents the initial peak intensity of the dye and A represents the peak intensity during the process. In this way, the degradation rate of MO by P25 reached 97% after 150 min, which is comparable to that obtained for P25 in a previous investigation.[27]

To our great surprise, a quite different result was observed for the BFO nanoparticles prepared in this study when they were employed to degrade the 10 mg per L MO solution through magnetic stirring. As shown in Fig. 2b, the absorption peak at
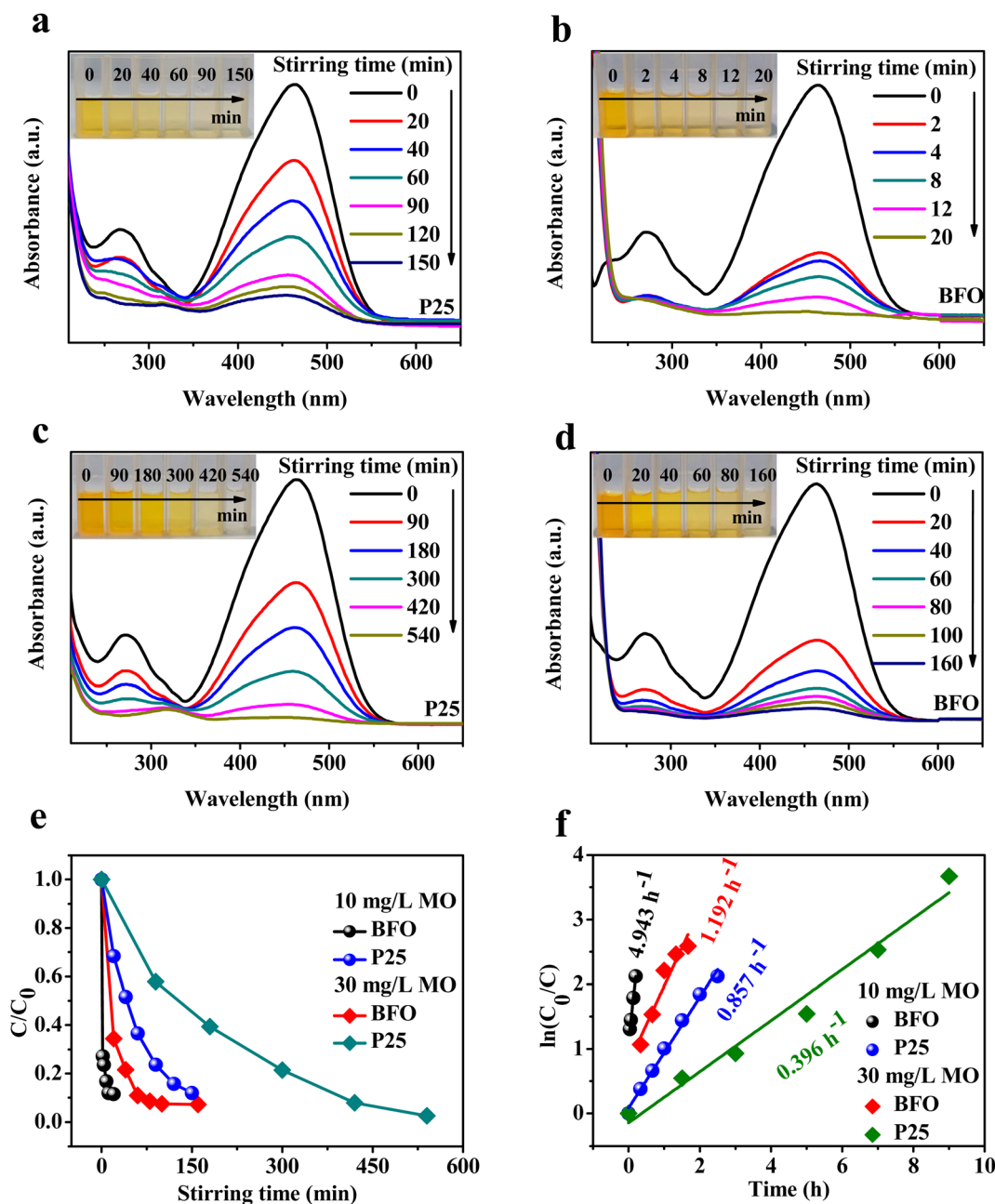

Fig. 2 Ultraviolet-visible absorption spectra of MO at different concentrations (inset: color contrast): (a) P25 10 mg L^{-1}, (b) BFO 10 mg L^{-1}, (c) P25 30 mg L^{-1}, and (d) BFO 30 mg L^{-1}. (e) Degradation rates and (f) kinetics curves of BFO and P25 powders at 10 mg L^{-1} and 30 mg L^{-1} concentrations.

464 nm completely disappeared, and the solution became completely colorless after only 20 min of magnetic stirring. Evidently, compared with P25, the BFO nanoparticles exhibited exceptionally outstanding capability in tribocatalytic degradation of MO solution.

It is well known that organic dyes at higher concentrations are more difficult to degrade.[25,31,32] Therefore, it is interesting to further explore the tribocatalytic degradation of 30 mg per L MO solutions by the BFO nanoparticles. For reference, P25 was employed to degrade 30 mg per L MO first, and the result is shown in Fig. 2c. Notably, 97% of 30 mg per L MO was degraded by P25 after 540 min of magnetic stirring. Undoubtedly, 30 mg per L MO was much more difficult to degrade by P25 than 10 mg per L MO. The same result was observed for the BFO nanoparticles, which degraded 99% of 30 mg per L MO after 160 min of magnetic stirring, as shown in Fig. 2d. Although 30 mg per L MO was much more difficult to degrade by the BFO nanoparticles than 10 mg per L MO, this should be the most efficient degradation of concentrated MO solutions as per our knowledge.[14,31,32,36] In a recent study on commercial 5 nm TiO_2 nanoparticles, DXN RT-30, the TiO_2 nanoparticles degraded 98.2% of 20 mg per L MO in 330 min[17], which was an highly exceptional finding. In another study on the tribocatalytic degradation of 30 mg per L MO by Si single crystals, although the solution became colorless after 120 min of magnetic stirring, MO molecules were only broken into smaller molecules such as benzoic acid, succinic acid, and p-phenol,[27] which were still harmful to the ambient environment. Therefore, a comparison of the degradation efficiency and catalytic mechanism of different catalysts for different dyes was conducted, as presented in Table 1.

The relationship curves between the degradation rates of 10 mg L^{-1} and 30 mg L^{-1} MO solutions treated with P25 and BFO nanoparticles and the magnetic stirring time are shown in Fig. 2e. For both MO solutions, the BFO nanoparticles exhibited a rather remarkable advantage over P25 in their degradation. On the basis of these curves, we developed an initial kinetic model to characterize the degradation efficiency of MO. As depicted in Fig. 2f, for MO solutions with concentrations of 10 mg L^{-1} and 30 mg L^{-1}, the frictional catalytic degradation rate constants of P25 were 0.857 h^{-1} and 0.396 h^{-1}, respectively, while the degradation rate constants of BFO were 4.943 h^{-1} and

1.192 h^{-1}, respectively. The latter values show a 5.76- and 3.01-fold difference from the former values.

In order to examine the frictional catalytic effect of BFO on other dyes, the frictional catalytic degradation of methylene blue was conducted, as depicted in Fig. 3. From the ultraviolet-visible absorption peak, it can be observed that after 13 h, the degradation rate reached 90%, which was lower than that for methyl orange. The degradation of methylene blue indicates the universality of the BFO nanofriction catalysts prepared using the sol–gel method in the degradation of organic dyes, eliminating the reliance on a single dye type. This result is comparable to the reported degradation of methylene blue by P25, where Mao *et al.* reported that P25 friction catalyzed degradation of MB (30 mg L^{-1}) occurred within 850 minutes at a degradation rate of 85%.[17] From the fitted reaction rate constant, the deviation of the intermediate point is related to the special catalytic process of BFO and methyl blue, namely the process from 3 to 7 h, during which no degradation was observed. This is probably related to dynamic physical adsorption saturation.[16] A similar phenomenon also occurred when DXN-RT30 (5 nm TiO_2) degraded methylene blue.[17] The result in Fig. 3c indicates that the frictional catalytic rate constant for MB degradation by BFO frictional catalysis was 0.126, which is lower than that for MO. This is also the reason for the low degradation efficiency of MB.

To demonstrate the functioning of friction catalysis from multiple perspectives, solutions without stirring were sampled at the same time points, as shown in Fig. 4a. The results revealed that the MO dye containing BFO nanopowders was hardly degradable in the absence of stirring. In previous investigations, a modified Teflon magnetic stirring rod adorned with two rings was often used to examine the absorption of organic dyes by nanoparticles.[13,17,19] Similarly, a rubber-sealed magnetic stirring rod was used to stir a 30 mg per L MO solution containing BFO nanoparticles, as shown in Fig. 4b. The intensity of the peak at 464 nm initially decreased very quickly, then gradually decreased, and even after 8 h of magnetic stirring, 40% of the peak intensity remained. Compared with the results shown in Fig. 2d, it can be concluded that for a concentrated MO solution, the concentration of MO molecules in the solution can be quickly decreased by BFO nanoparticles through adsorption. However, only through

Table 1 The list of friction efficiency and friction mechanisms of different catalysts

Catalyst	Organic dye	Mechanism	Friction Stimulation/speed	Degradation rate/time	Ref.
$Ba_{0.75}Sr_{0.25}TiO_3$	MO (5 mg L^{-1})	Electron transition	One PTFE rod/300 rpm	100%/24 h	19
GaN	MO (20 mg L^{-1})	Electron transition	Teflon magnetic disk/400 rpm	14%/24 h	38
TiO_2	MB (20 mg L^{-1})	Electron transition Al_2O_3	Teflon magnetic disk/400 rpm	93.1%/250 min	27
$SrTiO_3$	RhB (5 mg L^{-1})	Electron transfer	One PTFE rod/800 rpm	88.6%/24 h	24
CdS	MO (20 mg L^{-1})	Electron transition	Teflon magnetic disk/400 rpm	72%/24 h	29
Bi_2WO_6	RhB (5 mg L^{-1})	Electron transfer	Two PTFE rods/500 rpm	91%/12 h	25
CdS	RhB (5 mg L^{-1})	Electron transition	Four PTFE rods/—	99%/14 h	29
$Sr_{0.3}Ba_{0.7}TiO_3$	MO (10 mg L^{-1})	Electron transition	—	96%/12 h	28
ZnO_2		—	Teflon magnetic disk/400 rpm	90%/5 h	37
$NiCo_2O_4$					18
$BiFeO_3$	MO (30 mg L^{-1})	Electron transition	Teflon magnetic disk/400 rpm	99%/160 min	This work

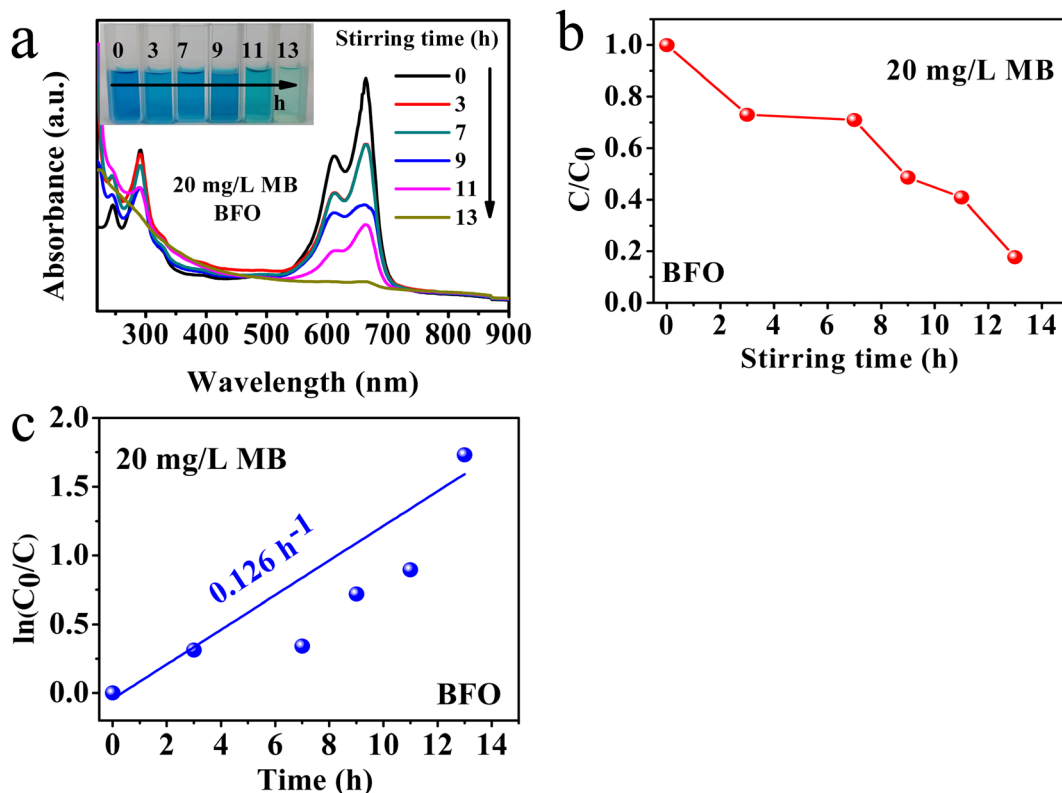© 2025 The Author(s). Published by the Royal Society of Chemistry

Fig. 3 (a) Ultraviolet-visible absorption spectra of methylene blue (MB) (inset color contrast), (b) degradation rate and (c) kinetics curves.

tribocatalysis can MO molecules be thoroughly removed from the solution.

In the friction catalytic process, a polytetrafluoroethylene circular turntable is used instead of a polytetrafluoroethylene magnetic rod, and friction-catalytic efficiency is improved. The results indicated that the greater the number of magnetic stirring rods, the larger the contact area and the higher the efficiency of dye degradation.[16,25] When the size of the stirring rods was determined, the stirring speed of the magnets also played a decisive role. Generally, the degradation efficiency of friction catalysis at a medium stirring rate was superior to that at low

speed.[13,16] The above results fully illustrate the crucial role of friction in the degradation process (Table 2).

The recyclability and stability, regarded as a major indicator for evaluating catalysts, the recyclability result for BFO as a friction catalyst for degrading methyl orange is presented in Fig. 5. As can be seen from the data in the figure, the degradation rate for BFO nanopowder for the first time was 99.12%, and the degradation rates for the subsequent four times were 92.26%, 81.43%, 63.45%, and 90%. With the increase in the number of cycles, the degradation rate slightly decreased. On the one hand, it is somewhat related to the loss of powder in the
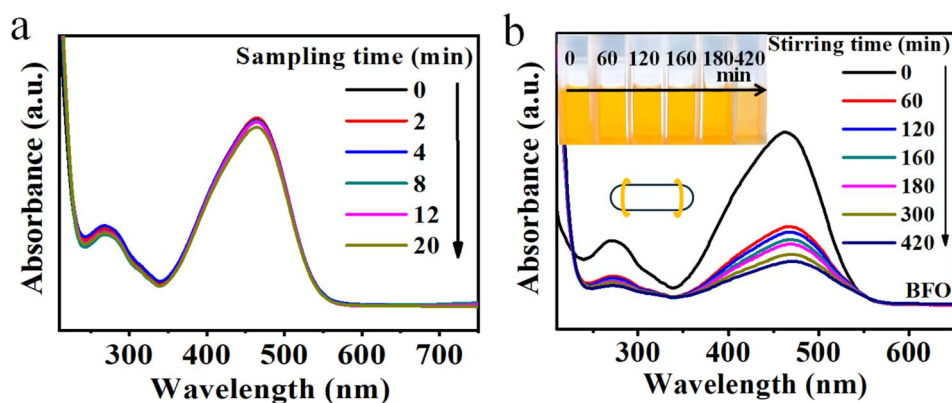

Fig. 4 The color and UV-visible adsorption spectra evolution of BFO nanoparticles (a) MO (10 mg per L) without agitation (b) MO (30 mg per L) under stirring using a rubber-sealed stirring rod.

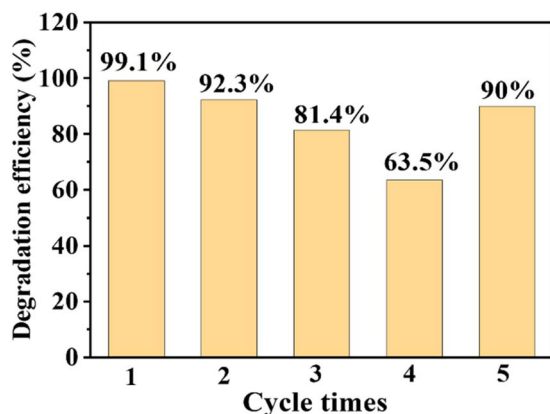| Full name	BiFeO$_3$	Methyl orange	TiO$_2$ nanoparticles	5 nm TiO$_2$ nanoparticles
Abbreviations	BFO	MO	P25	DXN RT-30

Fig. 5 The process cycle diagram of the tribocatalytic degradation of methyl orange by BFO nanopowders.

degradation process; on the other hand, it has a certain relationship with the structural stability of the powder. XRD results after five cycles of testing indicate that the XRD peaks of iron oxide are detected in the BFO powder after the fifth cycle, suggesting the generation of new substances during the friction process. Further in-depth studies are underway.

The band structures and bandgap widths of BFO and P25 were analyzed. The UV-visible absorption spectra of the BFO and P25 nanoparticles are presented in Fig. 4a. It is evident that with a decreasing wavelength, absorption abruptly increases at 678 nm for BFO and at 400 nm for P25, which are consistent with previously reported data.[6,33] The Tauc plot was employed to perform a linear extrapolation of $(\alpha h v)^2$ (α: absorption coefficient; h: Planck's constant; v: frequency of incident light) to zero, allowing for the determination of optical bandgap values for BFO and P25 nanoparticles, which were found to be approximately 1.9 and 3.24 eV, respectively, as depicted in Fig. 4b. These values are typical for BFO and P25. According to

the electron transition mechanism for tribocatalysis,[4,17] electron–hole pairs are excited in semiconductors by the mechanical energy absorbed through friction. Furthermore, the position of the valence band directly determines the oxidation ability of the vacancies located in the valence band; this indicates that the larger the position, the stronger the oxidation ability of the holes at that position. The position of the conduction band determines the reduction ability of electrons.[14,19] Therefore, considering the overall band transition mechanism, on the basis of satisfying the band electron transition, the larger the valence band position, the stronger the oxidation ability of the holes. The valence band position of BFO is approximately 1.75 eV *vs.* NHE, while that of P25 is 3.0 eV *vs.* NHE.[13,15] However, the wide bandgap of P25 limits the generation of electrons and holes, affecting its frictional catalytic efficiency. With a much smaller bandgap, BFO will have more electron–hole pairs excited than P25, which should explain its much better tribocatalytic degradation of MO than that of P25 (Fig. 6).

After electron–hole pairs are excited in BFO, they diffuse to the surface of the nanoparticles and induce various subsequent reactions. Experiments were carried out to investigate the main active species responsible for degrading MO solutions using BFO nanoparticles. As shown in Fig. 7, the inhibitory effects of TBA, BQ, and EDTA-2Na on the degradation of methyl orange by BFO are 10.8%, 17.5%, and 95.1%, respectively, while the inhibitory effect of AgNO$_3$ is almost negligible. It is well known that BQ, EDTA-2Na, TBA, and AgNO$_3$ capture $\cdot O^{2-}$ radicals, h$^+$ holes, $\cdot$OH radicals, and e$^-$ electrons, respectively. Obviously, positive holes are by far the most active species in the tribocatalytic degradation of methyl orange by BFO.

The mechanism of friction catalysis is likely similar to that of photocatalysis. The semiconductor materials involved in friction catalysis are typically narrow-bandgap semiconductors. Friction, as a kind of mechanical energy, and the catalyst, which
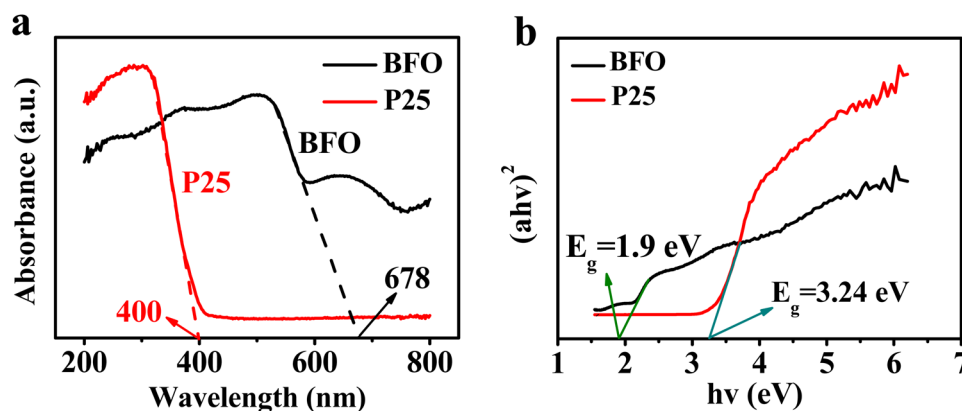

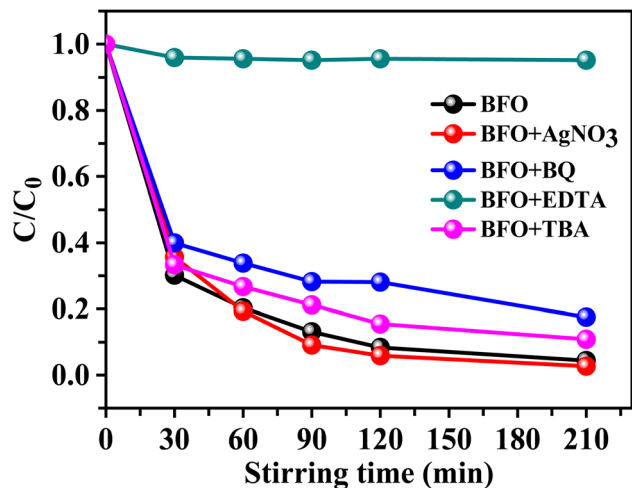**Fig. 6** (a) p25 and BFO UV absorption; (b) calculated bandgap plots.

Fig. 7 Effects of different free radical scavengers on the tribocatalytic degradation of MO by BFO nanoparticles.

is generally a semiconductor material, promotes the electrons of the catalyst to jump from the valence band to the conduction band during the friction process, thereby generating holes in the valence band and electrons in the conduction band. These electrons and holes participate in redox reactions that facilitate the degradation of dyes. For the tribocatalytic degradation of MO by TiO_2 nanoparticles, it has been shown that h^+, e^-, $\cdot OH$, and $\cdot O_2^-$ all participate in the degradation of MO molecules within the solution, which can be expressed as follows:[17]

$$h^+/e^-/\cdot OH/\cdot O^{2-} + MO \rightarrow degradation \qquad (1)$$
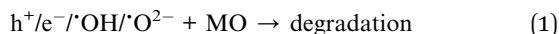
However, according to the radical capturing results shown in Fig. 5, holes are mostly responsible for the degradation of MO in this study, which can be expressed as follows:
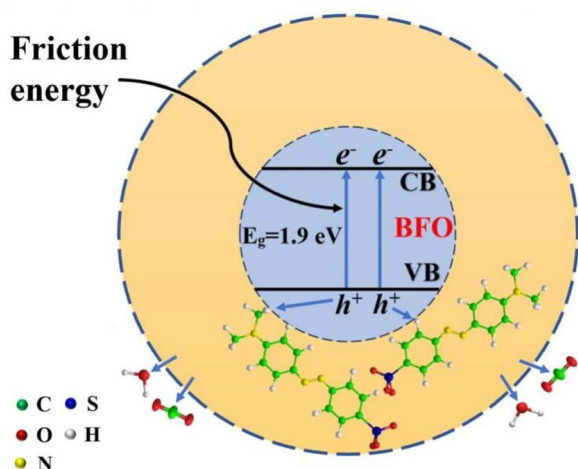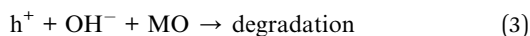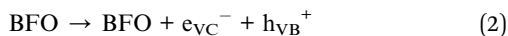
$$BFO \rightarrow BFO + e_{VC}^- + h_{VB}^+ \qquad (2)$$

$$h^+ + OH^- + MO \rightarrow degradation \qquad (3)$$

Fig. 8 Mechanism diagram of the friction catalytic effect of BFO powder.

Fig. 8 presents a schematic of the process of tribocatalytic degradation of MO by BFO nanoparticles. Two points are worthy to be emphasized: one is that the bandgap (1.9 eV) is relatively narrow, which accounts for the exceptional tribocatalytic degradation of MO by BFO. The other is that holes have been found by far the most active species in the tribocatalytic degradation of methyl orange by BFO, and the reaction of holes and MO molecules is highlighted in Fig. 8.

4. Conclusions

As a branch of mechanochemistry, friction catalysis exhibits vast application prospects in dye degradation, water pollution governance, and environmental restoration. BFO nanoparticles prepared *via* the sol–gel method demonstrated significant mechanical degradation capability in 10 mg per L and high-concentration 30 mg per L MO solutions. At a Teflon disk rotation speed of 400 rpm, under dark and room temperature conditions, the BFO nanoparticles exhibited degradation rates of 99% and 100% for MO at concentrations of 10 mg per L and 30 mg per L within 20 minutes and 160 minutes, respectively. These results can be attributed to the appropriate crystallite size (≈ 150 nm), crystallinity, and suitable bandgap width (1.9 eV) of the BFO nanoparticles. The BFO nanoparticles exhibited pronounced physical adsorption characteristics toward MO dye molecules. Based on the results of the active substance capture experiment, it is hypothesized that the degradation of MO molecules is primarily facilitated by the action of h^+ ions. This study not only underscores the significant potential of BFO nanoparticles prepared using the sol–gel method for environmental remediation, but also promotes the advancement of more sophisticated friction catalysts.

Data availability

The data that support the findings of this study are available from the corresponding author upon reasonable request.

Author contributions

Conflicts of interest

The authors declare that all the authors have no competing financial interests or personal relationships that influence the work reported in this article.

Acknowledgements

References

1 P. Anand, D. P. Jaihindh, W. K. Chang and Y. P. Fu, *Appl. Surf. Sci.*, 2021, **540**, 148387.

2 Y. Wang, S. Shen, M. Liu, G. He and X. Li, *Colloid Interface Sci.*, 2024, **655**, 187–198.

3 Z. Wang, X. Xuanli Dong, W. Tang and Z. L. Wang, *Chem. Soc. Rev.*, 2024, **53**, 4349–4373.

4 X. Li, W. Tong, J. Shi, Y. Chen, Y. Zhang and Q. An, *J. Mater. Chem. A*, 2023, **11**, 4458–4472.

5 A. Soam, R. Kumar, M. Singh, D. Thatoi and R. O. Dusane, *J. Alloys Compd.*, 2020, **813**, 152145.

6 Y. Zhu, C. Quan, Y. Ma, Q. Wang, W. Mao, X. Wang, J. Zhang, Y. Min, J. Yang and X. a. Li, *Mater. Sci. Semicond. Process.*, 2017, **57**, 178–184.

7 A. Gaur, C. Porwal, V. S. Chauhan and R. Vaish, *J. Am. Ceram. Soc.*, 2024, **107**, 2393–2406.

8 Z. Li, Y. Xie, Y. Wang, Y. Peng, Z. Deng, B. Liu, G. Zhang, X. Wang, F. Zhang and L. Zhu, *J. Solid State Chem.*, 2023, **317**, 123707.

9 A. Dhawan, A. Sudhaik, P. Raizada, S. Thakur, T. Ahamad, P. Thakur, P. Singh and C. M. Hussain, *J. Ind. Eng. Chem.*, 2023, **117**, 1–20.

10 P. Banoth, C. Kandula, P. K. Lavudya, S. Akaram, L. De Los Santos Valladares, R. Ammanabrolu, G. K. Mamidipudi and P. Kollu, *ACS omega*, 2023, **8**, 18653–18662.

11 M. Ghorbani, S. Sheibani, H. Abdizadeh and M. R. Golobostanfard, *J. Mater. Res. Technol.*, 2023, **22**, 1250–1267.

12 F. Gao, X. Chen, K. Yin, S. Dong, Z. Ren, F. Yuan, T. Yu, Z. Zou and J. Liu, *Adv. Mater.*, 2007, **19**, 2889–2892.

13 H. Lei, M. Wu, F. Mo, S. Ji, X. Dong, Z. Wu, J. Gao, Y. Yang and Y. Jia, *Nano Energy*, 2020, **78**, 105290.

14 L. V. Trandafilović, D. J. Jovanović, X. Zhang, S. Ptasińska and M. Dramićanin, *Appl. Catal., B*, 2017, **203**, 740–752.

15 S. Fang and Y. H. Hu, *Soc. Rev.*, 2022, **51**, 3609–3647.

16 J. Zhao, F. Chen, W. Luo, H. Li, Z. Wu, Z. Xu, Y. Zhang, H. Zhang, G. Yuan and J. Gao, *Ceram. Int.*, 2020, **46**, 25293–25298.

17 C. Mao, H. Lei, Z. Guo, X. Jia, X. Cui, J. Huang, L. Fei, Y. Jia and W. Chen, *Ceram. Int.*, 2024, **50**, 4737–4745.

18 H. Lei, X. Cui, X. Jia, J. Qi, Z. Wang and W. Chen, *Nanomaterials*, 2022, **13**, 46.

19 P. Li, J. Wu, Z. Wu, Y. Jia, J. Ma, W. Chen, L. Zhang, J. Yang and Y. Liu, *Nano Energy*, 2019, **63**, 103832.

20 A. Gaur, C. Porwal, V. S. Chauhan and R. Vaish, *Sci.: Mater. Electron.*, 2023, **34**, 2154.

21 L. Geng, Y. Qian, W. Song and L. Bao, *Appl. Surf. Sci.*, 2023, **637**, 157960.

22 B. Yang, H. Chen, Y. Yang, L. Wang, J. Bian, Q. Liu and X. Lou, *J. Mater. Chem. C*, 2021, **416**, 128986.

23 X. Li, W. Tong, W. Song, J. Shi and Y. Zhang, *J. Cleaner Prod.*, 2023, **414**, 137566.

24 J. Cao, Y. Jia, X. Wan, B. Li, Y. Zhang, S. Huang, H. Yang, G. Yuan, G. Li and X. Cui, *Ceram. Int.*, 2022, **48**, 9651–9657.

25 M. Wu, H. Lei, J. Chen and X. Dong, *J. Colloid Interface Sci.*, 2021, **587**, 883–890.

26 M. Wu, Y. Zhang, Y. Yi, B. Zhou, P. Sun and X. Dong, *J. Hazard. Mater.*, 2023, **459**, 132147.

27 X. Cui, P. Li, H. Lei, C. Tu, D. Wang, Z. Wang and W. Chen, *Sep. Purif. Technol.*, 2022, **289**, 120814.

28 C. Mao, Y.-C. Zhang, H. Lei, X. Jia, F. Chen, W. Yao, P. Liu and W. Chen, *Appl. Surf. Sci.*, 2024, **663**, 160172.

29 A. Lima, *J. Phys. Chem. Solids*, 2020, **144**, 109484.

30 H. You, Z. Wu, L. Zhang, Y. Ying, Y. Liu, L. Fei, X. Chen, Y. Jia, Y. Wang and F. Wang, *Angew. Chem., Int. Ed.*, 2019, **131**, 11905–11910.

31 A. Ranjbari, J. Kim, J. Yu, J. Kim, M. Park, N. Kim, K. Demeestere and P. M. Heynderickx, *Catal. Today*, 2024, **427**, 114413.

32 A. Hojjati-Najafabadi, E. Farahbakhsh, G. Gholamalian, P. Feng, F. Davar, T. M. Aminabhavi, Y. Vasseghian, H. Kamyab and H. Rahimi, *J. Water Process Eng.*, 2024, **59**, 105002.

33 J.-H. Xu, H. Ke, D.-C. Jia, W. Wang and Y. Zhou, *J. Alloys Compd.*, 2009, **472**, 473–477.

34 K. Nakata and A. Fujishima, *J. Photochem. Photobiol., C*, 2012, **13**, 169–189.

35 M. Rafique, S. Hajra, M. Irshad, M. Usman, M. Imran, M. A. Assiri and W. M. Ashraf, *ACS Omega*, 2023, **8**, 25640–25648.

36 Y. Zhu, J. Ren, G. Huang, C. L. Dong, Y. C. Huang, P. Lu, H. Tang, Y. Liu, S. Shen and D. Yang, *Adv. Funct. Mater.*, 2024, **34**, 2311623.

37 X. Xu, C. Mao, J. Song, S. Ke, Y. Hu, W. Chen and C. J. M. Pan, *Materials*, 2024, **17**, 3487.

38 H. Lei, X. Cui, X. Jia, J. Qi, Z. Wang and W. J. N. Chen, *Nanomaterials*, 2022, **13**, 46.